

Article type: Full Paper

Amorphous Quantum Nanomaterials

*Ferdinand F. E. Kohle, Joshua A. Hinckley, Songying Li, Nikhil Dhawan, William P. Katt, Jacob A. Erstling, Ulrike Werner-Zwanziger, Josef Zwanziger, Richard A. Cerione, Ulrich B. Wiesner**

Dr. F. F. E. Kohle, J. A. Hinckley, S. Li, N. Dhawan, Prof. U. B. Wiesner
Department of Materials Science and Engineering, Cornell University, Ithaca, NY 14853, USA.
Email: ubw1@cornell.edu

Dr. F. F. E. Kohle, J. A. Hinckley, Prof. R. A. Cerione
Department of Chemistry and Chemical Biology, Cornell University, Ithaca, NY 14853, USA.

Dr. W. P. Katt, Prof. R. A. Cerione
Department of Molecular Medicine, Cornell University, Ithaca, NY 14853, USA.

J. A. Erstling
Department of Biomedical Engineering, Cornell University, Ithaca, NY 14853, USA.

Dr. U. Werner-Zwanziger, Prof. J. Zwanziger
Department of Chemistry, Dalhousie University, Halifax, Nova Scotia B3H 4R2, Canada.

Keywords: amorphous silica nanoparticles, organic dyes, photodynamic therapy (PDT), optical super-resolution microscopy

In quantum materials macroscopic behavior is governed in non-trivial ways by quantum phenomena. This is usually achieved by exquisite control over atomic positions in crystalline solids. Here we demonstrate that the use of disordered glassy materials provides unique opportunities to tailor quantum material properties. By borrowing ideas from single molecule spectroscopy, we isolate single delocalized π -electron dye systems in relatively rigid ultrasmall (<10nm diameter) amorphous silica nanoparticles. We demonstrate that chemically tuning the local amorphous silica environment around the dye over a range of compositions enables exquisite control over dye quantum behavior, leading to efficient probes for photodynamic therapy (PDT) and stochastic optical reconstruction microscopy (STORM). Results suggest that efficient fine-tuning of light-induced quantum

behavior mediated via effects like spin-orbit coupling can be effectively achieved by systematically varying averaged local environments in glassy amorphous materials as opposed to tailoring well-defined neighboring atomic lattice positions in crystalline solids. Resulting nanoprobe features have been proven to enable clinical translation.

In quantum materials macroscopic behavior, typically under the influence of external fields (e.g. magnetic fields or electromagnetic fields), is dictated in nontrivial ways by quantum phenomena.^[1] Prototypical examples are semiconductor quantum dots (Q dots, **Figure 1a**). It was long known that semiconductors exhibit a material dependent band gap. But it took until the 1980's to demonstrate that at nanoscopic length scales this band gap is sensitive to confinement effects leading to exquisitely tunable optical (absorption/emission) properties of Q dots under illumination.^[2] Besides spatial confinement, other phenomena in quantum materials include quantum fluctuations, quantum entanglement, quantum coherence, or relativistic spin-orbit coupling. Their tuning to control macroscopic materials behavior usually involves the crystalline state where lattice parameters (e.g. by strain engineering via epitaxial relations) and/or lattice symmetry provide specific experimental “knobs” controlling interactions at the atomic level.^[3,4,5]

The use of disordered glassy materials to harness quantum phenomena is much less common but offers intriguing opportunities.^[6] For example, silica glasses allow large variations in composition without changing the amorphous nature of the solid state.^[7] Borrowing ideas from single molecule spectroscopy in condensed matter (polymer) matrices,^[8] here we introduce the idea of tuning quantum phenomena to control macroscopic behavior under illumination of ultrasmall (<10 nm diameter) amorphous silica nanoparticles (SNPs) encapsulating isolated conjugated π -electron systems in the form of single organic dye molecules. SNPs are modified

with aluminum as a network hardener and are surface-functionalized with polyethylene glycol (PEG) for colloidal stability in aqueous solutions (see Supporting Information). We demonstrate that chemically tuning the local amorphous silica environment over a range of compositions enables exquisite control over quantum behavior of the π -electron system of the dyes (Figure 1b): Co-condensing increasing amounts of the heavy element iodine bearing precursors into the ultrasmall SNPs enables control of the strength of spin-orbit coupling to systematically enhance dye intersystem crossing (ISC, *i.e.* singlet-triplet transition) rates from singlet to triplet quantum states. This provides *e.g.* highly efficient photosensitizers for applications like photodynamic therapy. Silica functionalization with increasing numbers of thiol groups enables fine-tuning of light-induced on-off switching of dye dark states providing ultrabright and efficiently blinking nanoprobe for optical super-resolution (SR) microscopy. We will refer to these materials as amorphous quantum (nano)materials (AQNs or AQMs). We expect these concepts will stimulate research on a range of quantum phenomena in amorphous solid-state materials systems.

AQNs with controlled dye triplet populations: We utilized spin-orbit coupling induced by high atomic number Z elements, *i.e.* iodine, to finely tune the triplet state population of carbonyl rhodamine dye ATTO647N covalently encapsulated in amorphous matrices of SNPs (Figure 1c). ISC is a spin-forbidden transition usually suppressed, but is enhanced by spin-orbit coupling, which is observed for molecules in the proximity of high Z atoms.^[9,10] This makes iodine loaded particles attractive candidates *e.g.* for applications in photodynamic therapy (PDT)^[11] or SR optical microscopy, such as ground-state depletion (GSD) microscopy.^[12]

We varied the chemical composition of sub-10 nm SNPs beneficial for biological applications synthesized in water (referred to as C' dots) utilizing a silica growth quenching

mechanism.^[13,14] We prepared iodine containing C' dots (iC' dots) covalently encapsulating a single ATTO647N dye per particle from assorted silica molar precursor ratios of (3-iodopropyl)trimethoxysilane (IPTMS) to tetramethylorthosilicate (TMOS): 0%, 1%, 2.5%, 5%, 7.5%, 10%, and 20% iC' dots. Unreacted precursor was separated from the particles by dialysis and gel permeation chromatography (GPC). Figure 1d shows the ATTO647N intensity-matched UV-vis spectra of this particle series in deionized water. Spectra exhibited the 647 nm absorption of ATTO647N, as well as a 255 nm UV absorption band which increased with increasing IPTMS precursor amount, matching a band from pure IPTMS recorded in 100% anhydrous ethanol to avoid precursor condensation. Iodine was independently evidenced by EDS measurements on 0%, 5%, and 20% iC' dots (Figure S1).

Particle hydrodynamic diameters, d_{sample} , dye numbers per particle, and dye triplet state populations were determined by fluorescence correlation spectroscopy (FCS, Figure 1e, and S2a), employing a fit model that accounts for translational diffusion, ISC, and rotational diffusion (see Supporting Information, equations 1 and 2).^[15,16] All diameters were below 9 nm (Figure 1f, Table S1), and increased roughly linearly with increasing IPTMS ratio. As desired, the number of ATTO647N dyes ($\epsilon = 150000 \text{ M}^{-1} \text{ cm}^{-1}$) per particle stayed close to $n=1$ over the entire series (Table S1) and the number of iodopropyl groups ($\epsilon \approx 1900 \text{ M}^{-1} \text{ cm}^{-1}$, Figure S2b) increased linearly (Figure 1h). However, deriving the iodopropyl-group density from the estimated particle volume (Figure 1g) and number of iodopropyl groups (Figure 1h), reveals an asymptotic approach towards a maximum of around 1 functional group per three cubic nanometers (Figure 1i).

The effects of iodine on the singlet-to-triplet transitions of ATTO647N were studied using an afterpulse-corrected FCS setup (Figure S2).^[17] Continuously increasing triplet

populations as a function of iodopropyl-group content are manifested by increases in amplitudes of fast processes at lag times between ~ 100 ns and $10 \mu\text{s}$,^[15,18] as clearly revealed by FCS results in Figure 1e. In Figure 1j, the %-triplet population for iC' dots as derived from FCS fits strongly increases between 0% and 10% IPTMS and then saturates, amounting to an increase of about 600% relative to iodine free C' dots. The triplet population hence follows the iodopropyl-group density in a particle (Figure 1i). As expected, the fluorescence brightness per dye, as revealed by FCS determined particle brightness, simultaneously decreases to about a fourth of its initial value (Figure 1k). Results demonstrate that similar to biological systems,^[19,20] in these AQNs amorphous silica matrices allow efficient control over the strength of relativistic spin-orbit coupling enabling fine-tuning of light-induced quantum states of encapsulated dyes by means of varying compositionally averaged local environments as opposed to well-defined neighboring atomic lattice positions in crystalline materials (Figure 1j).

An increase in triplet state dye population is often associated with an increase in singlet oxygen ($^1\text{O}_2$) quantum yield, Φ_Δ .^[21,22] $^1\text{O}_2$ is produced by energy transfer between the triplet state dye and dissolved triplet oxygen, $^3\text{O}_2$ (**Figure 2a and 2b**). Using this mechanism transitions ultrasmall SNPs from diagnostic (passive) to therapeutic (active) probes, *e.g.* applicable for PDT, where a targeted probe with high Φ_Δ would specifically bind to biological sites of interest, be excited with light to produce $^1\text{O}_2$, and induce cell death (Figure 2b).^[11] Working with ultrasmall SNPs that have already been FDA approved as an investigational new drug (IND) for human clinical trials may be particularly beneficial.^[23]

We measured Φ_Δ for ATTO647N encapsulated in iC' dots by using the singlet oxygen sensor 1,3-diphenylisobenzofuran (DPBF), which forms 1,2-dibenzoylbenzene with $^1\text{O}_2$ (Figure 2c) as indicated by reduction of a 410 nm absorption band (Figure 2d and S3). Upon dye

encapsulation in 0% iC' dots, Φ_{Δ} slightly decreased as compared to free dye, likely due to steric shielding. However, values of Φ_{Δ} increased with increasing IPTMS concentration (Figure 2e, see Figure S3 for a sample calculation). While the maximum Φ_{Δ} value of 8.0% is much greater than that for ATTO647N alone (1.2%), it is far below the desired Φ_{Δ} of 50% for PDT applications.^[24] We therefore synthesized 0%, 7.5%, and 15% iC' dots replacing ATTO647N with methylene blue derivate MB2 (Figure 2f inset and Figure S4), with resulting MB2 Φ_{Δ} values up to 71% (Figure 2f, Table S2), and no signs of dark toxicity ($^1\text{O}_2$ generation in the absence of light, Figure S5). This places MB2 dye encapsulated in iC' dots in the range of top-performing photosensitizers,^[24] while simultaneously enabling surface functionalization with, *e.g.* targeting moieties and radiolabels providing multifunctional nanoprobes.^[25] Finally, we investigated the ability to co-localize multiple MB2 dyes in one particle ($n>1$) and measured the apparent singlet oxygen quantum yield of a particle, $\Phi_{\Delta}^{\text{app}}$ (dye multiplicity effect). For that purpose, we synthesized PEGylated and tetramethylrhodamine (TMR) dye surface-functionalized sub-10 nm MB2 encapsulating SNPs (C' dots, *i.e.* without iodopropyl groups), enabling an estimation of particle concentration, size, and number of MB2 dyes per particle by FCS not possible without TMR (Figure S6).^[25] Measurements yielded an $\Phi_{\Delta}^{\text{app}}$ of 114% (Figure 2f). With an estimated number of 2.9 MB2 dyes per particle, this comprises an estimated Φ_{Δ} contribution of each MB2 dye of about 39% to $\Phi_{\Delta}^{\text{app}}$. We expect the combination of both approaches (not tested here), *i.e.* iodine-based spin-orbit coupling induced increases in Φ_{Δ} and multiplicity effects to maximize $\Phi_{\Delta}^{\text{app}}$ to create ultra-potent PDT probes. To our knowledge these are the smallest PEGylated SNPs for PDT reported to date.

AQNs with controlled dye dark states: We also tested the concept of tuning dye quantum

behavior by varying compositionally averaged local silica environments using photochemistry approaches. To that end, we synthesized photoswitchable sub-10 nm Cy5 containing SNPs, by enriching the silica matrix with mercapto groups. In the presence of primary thiols in solution, *e.g.* in form of imaging buffer additives such as β -mercaptoethanol (β ME), Cy5 is known to undergo photo-conversion between bright and long-lived dark states by forming a Cy5-thiol adduct (**Figure 3a**),^[26-28] enabling *e.g.* stochastic optical reconstruction microscopy (STORM).^[29] However, while additives such as β ME support favorable emissive behavior, they typically compromise cell integrity or are otherwise incompatible with experimental conditions.^[30,31] Furthermore, mercapto compounds have very characteristic smells, making them unpleasant to work with.

Four different mercapto group containing C' dots (super-resolution C' dots, srC' dots) were synthesized from varying molar ratios of (3-mercaptopropyl) trimethoxysilane (MPTMS) and TMOS: 0%, 30%, 60%, and 80% srC' dots. FCS measurements yielded hydrodynamic diameters of less than 8 nm for all Cy5 srC' dots and showed that as desired the number of dyes per srC' dot stayed close to $n=1$ over the entire series (Figure 3b, Table S3). For the application of NPs in optical SR microscopy it is crucial to minimize particle diameters to prevent localization uncertainty and to optimize labeling efficiency. We therefore investigated size tunability of 60% srC' dots by quenching particle growth via PEG-silane addition at different reaction times.^[13] PEGylated particles as small as 5.2 nm were prepared (Figure S7, Table S3), approaching the size of fluorescent proteins (*e.g.* GFP with ~ 4 nm long-axis), to our knowledge providing the smallest PEGylated SNPs for super resolution microscopy to date.

Intensity-matched UV-vis spectra and respective fluorescence emission spectra of srC' dots and free Cy5 dye in deionized water at pH 7 are compared in Figure 3c. In contrast to free dye

and 0% srC' dots, all other srC' dots exhibited an additional absorption peak emerging around 245 nm and a shoulder around 300 nm. While the peak at 245 nm is likely a combination of the absorption of mercaptopropyl groups and PEG (Figure S8), the shoulder around 310 nm suggests a Cy5-thiol adduct. This adduct has been described in detail,^[26-28] and is a result of thiol binding to the polymethine bridge of Cy5. All particles showed a minor bathochromic shift of Cy5 absorption and emission peaks, and a per dye fluorescence brightness enhancement expected from Cy5 encapsulation into a rigid silica matrix.^[13] Enhancements have been shown to originate from an increase in radiative rate, a decrease in non-radiative rate, or both.^[13,16] The largest per dye brightness enhancement of 1.9 was observed for the control particle (0% srC' dots) and decreased slightly to 1.7 with increasing MPTMS/TMOS molar ratio (Figure 3c).

Since the much higher molar functionalization of silica in srC' dots as compared to iC' dots is expected to substantially alter the aluminosilicate network structure, we performed ²⁹Si, ²⁷Al, and ¹³C solid state NMR (ssNMR) experiments on 0%, 30%, and 60% srC' dots (see supplementary information for details). ²⁹Si ssNMR results (Figure 3d) were consistent with increased incorporation of MPTMS lowering the silica network density as demonstrated by increasing signals for oxygen tri-coordination of silicon (T-groups) versus quaternary coordination (Q-groups), corroborated by energy-dispersive X-ray spectroscopy (EDS, Figure S9). ²⁷Al ssNMR spectra (Figure 3e) primarily exhibited four-fold (tetrahedrally) coordinated aluminum, with aluminum atoms likely replacing silicon in the silica network, contributing to particle stabilization below the isoelectric point of SNPs during particle formation.^[13] Finally, solid-state CP/MAS ¹³C NMR measurements (Figure 3f) confirmed successful PEGylation of the srC' dots and revealed that the majority of sulfur containing moieties are mercaptopropyl groups, but also suggested oxidative formation of disulfide bonds during synthesis.^[32]

We next compared ensemble photoswitching behavior of srC' dots to free Cy5 dye. The Cy5-thiol adduct is formed by exposure to red light (633 nm), leading to a quenching of the primary Cy5-absorption band, and enhancement of a band at 310 nm. The adduct dissociates upon UV light (300 nm) irradiation (Figure 3a), leading to reduction of the 310 nm band and recovery of the primary band. **Figure 4a** shows the normalized absorption spectra for a SR imaging cocktail comprised of Cy5 dye and 140 mM β ME (Cy5- β ME), as well as for 0%, 30%, 60%, and 80% srC' dots without β ME. Upon 633 nm illumination of Cy5- β ME, the main 647 nm absorption peak decreases while a shoulder at 310 nm emerges. Subsequent exposure to 300 nm light partially restores the 647 nm peak, indicating partial photo-bleaching of some Cy5 molecules, and in agreement with previous observations.^[28] For 0% srC' dots, exposure to 633 nm light causes the 647 nm peak to substantially decrease, but without forming a significant peak at 310 nm. Subsequent exposure to 300 nm light cannot recover the primary peak, but instead further decreases it, indicating photo-bleaching. Thiol containing srC' dots also show the decrease of the 647 nm peak and unchanged shoulder at \sim 310 nm. However, under 300 nm UV exposure the shoulder absorption decreases and the main peak at 647 nm partially recovers, similar to the Cy5- β ME. The extent of recovery of srC' dots increases with increasing thiol content, suggesting that the mercapto-enriched silica matrix can fine-tune Cy5-thiol adduct formation either during the synthesis or upon 633 nm illumination or both.

To better understand the fluorescence characteristics of the particles, we analyzed them using total internal reflection fluorescence microscopy (TIRFM). We prepared Cy5-biotin and biotinylated 0% and 60% srC' dots (Figure S10h), immobilized each on streptavidin-coated glass surfaces, and compared srC' dots to immobilized Cy5-biotin with and without β ME cocktail via TIRFM. Figure 4b and 4c show three fluorescence time traces for each sample in PBS buffer

(see Supplementary Information and Figure S11). While Cy5 and 0% srC' dots bleach in a matter of seconds, Cy5- β ME and 60% srC' dots show fluorescence blinking behavior over the entire acquisition time. This suggests that the local thiol group concentration within these srC' dots enables encapsulated Cy5 to enter long-lived dark states. Similar results were obtained by replacing Cy5 with Cy3 (Figure 4d, 4e, and Figure S10g), but with blinking intensities of 60% Cy3 srC' dots substantially enhanced over Cy3-biotin dye. This is further reflected via photon histograms (Figure 4f to i). While Cy5 srC' dots show a factor of about 1.1 more photons per switching event than Cy5-biotin, this factor increases to 2.7 for Cy3. These factors are consistent with brightness enhancements as estimated by steady-state emission spectra of absorption matched samples of Cy3- and Cy5-biotin as compared to respective srC' dots (Figure S10 and Table S4). Since order of magnitude enhancement, via silica encapsulation, can be obtained for specific dyes (see results for DY782 dye in Figure S10c and Table S4), results suggest a path to ultrabright SR imaging probes.

Another important parameter to evaluate fluorescent probes for STORM is the on-off duty cycle.^[33] It should be low to minimize the probability that another probe fluoresces within the diffraction limited area to optimize image resolution according to the Nyquist criterion.^[34] Analysis yielded averages of 0.0003 for Cy5-biotin, Cy5 60% srC' dots, and Cy3-biotin, and 0.0007 for Cy3 60% srC' dots. These results place 60% srC' dots in the category of potent super-resolution fluorescent probes.^[33] Similar to the iC' dot case, taken together these results again demonstrate that varying compositionally averaged amorphous local silica environments enables precise fine-tuning of quantum phenomena in dye-encapsulating SNPs leading to controlled macroscopic behavior under light stimulation, here in the form of particle blinking statistics.

To illustrate the biological benefits of srC' dots, we compared the effects of 60% srC'

dots and β ME when applied to BxPC3 pancreatic cancer cells in complete media. **Figure 5a** shows relative cell viability for BxPC3 cells following 6 days of treatment with 60% srC' dots, versus only a 16-hour treatment with β ME. For meaningful comparison, the compound concentrations on the X-axis were scaled as 'fraction of imaging concentration'. This is the concentration typically reported for dye labeling (1 μ M for srC' dots used here),^[35] or for β ME in a typical STORM imaging cocktail (140 mM).^[28,33] At only 10% (*i.e.* 14 mM) of the typical imaging concentration for β ME, substantial cell death is observed after only 16 hours, while srC' dots were well tolerated for 6 days at nearly ten-fold a typical imaging concentration (*i.e.* 7.5 μ M).

For STORM data processing of TIRFM images we analyzed image stacks of biotinylated 60% srC' dots with the ImageJ plugin ThunderSTORM.^[36] Figure 5b shows an excerpt from a diffraction-limited TIRFM image with multiple localized srC' dots. The particles seem well resolved by TIRFM alone, but Figure 5c shows several particles only resolved via STORM analysis. This is demonstrated in Figure 5d, which zooms in on two particles unresolved by TIRFM, and the accompanying STORM reconstruction of these particles in Figure 5e. The inset of Figure 5e shows the corresponding cross-sectional line profiles of the diffraction limited TIRFM image (dashed line) and reconstructed STORM image (solid line) revealing a center-to-center particle distance of 175 nm. Corresponding analysis (Figure 5f) of localized particles for their full width half maximum (FWHM), shows a decrease from 215 ± 35 nm to 36 ± 6 nm. To demonstrate dual color STORM, we combined Cy5 (red) srC' dots and Cy3 (green) srC' dots for imaging (Figure 5g and 5h). Figure 5i to 5k demonstrate resolution enhancement by comparing TIRFM and STORM images of microtubules labeled with Cy5 60% srC' dots coated with amino-group-reactive N-hydroxysuccinimide (NHS) esters (see methods and SI). Figure 5j

shows a single microtubule while Figure 5k reveals multiple parallel microtubules only resolved via STORM.

In this work, we studied the effects of variations in average composition of glassy amorphous silica environments on tuning quantum state populations of only a few delocalized π -electron dye systems. While we examined a few different scenarios for sub-10 nm silica nanoparticles, we anticipate that these findings will stimulate research and development activities on a range of quantum phenomena in other amorphous solid-state materials and in a number of communities. To our knowledge, the particles described in this study present the smallest colloidally stable silica nanoparticles for stochastic optical reconstruction microscopy and photodynamic therapy to date that fulfill necessary requirements for clinical translation.^[23] The work therefore opens a realistic pathway to push advances in the physical sciences into the clinical space.

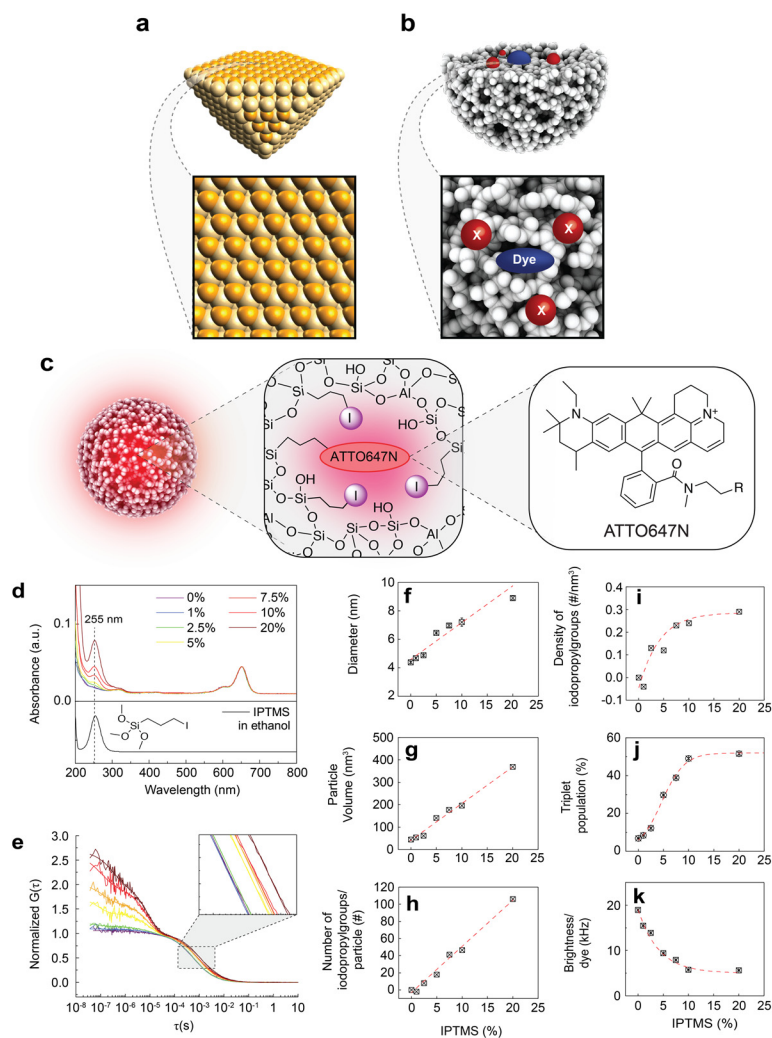


Figure 1. (a) Comparison of highly ordered atomic positions in a cadmium selenide quantum dot with atomic disorder in a (b) amorphous silica nanoparticle, both sub-10 nm, with encapsulated delocalized π -electron dye system and silica compositional modifications X (here iodine or sulfur atoms) that tune the quantum photophysical dye behavior under illumination. (c) ATTO647N particle rendering with local molecular structure model and chemical structure of encapsulated ATTO647N. R represents a functional group attached by a carbon atom. (d) Comparison of absorption spectra of ATTO647N iC' dots in water (top), synthesized from different relative molar amounts of (3-iodopropyl) trimethoxysilane (IPTMS) precursor (0, 1, 2.5, 5, 7.5, 10, and 20%), and of IPTMS in ethanol (bottom, inset shows chemical structure of IPTMS). (e) Normalized afterpulse-corrected FCS autocorrelation curves of ATTO647N iC' dots from (d). Fits used a correlation function with translational diffusion, singlet-triplet transition, and rotational diffusion components. Inset shows enlarged correlation curves with fits. (f) Diameter from FCS fits plotted against IPTMS precursor amount. (g) Particle volume as calculated from particle diameter. (h) Number of iodopropyl groups as determined from a combination of FCS and absorption measurements. (i) Estimated iodopropyl group density as obtained from data in (g) and (h). (j)

Triplet population plotted against IPTMS precursor amount. (k) FCS derived brightness per dye plotted against IPTMS precursor amount. Red dotted lines in (f-k) serve as visual guides.

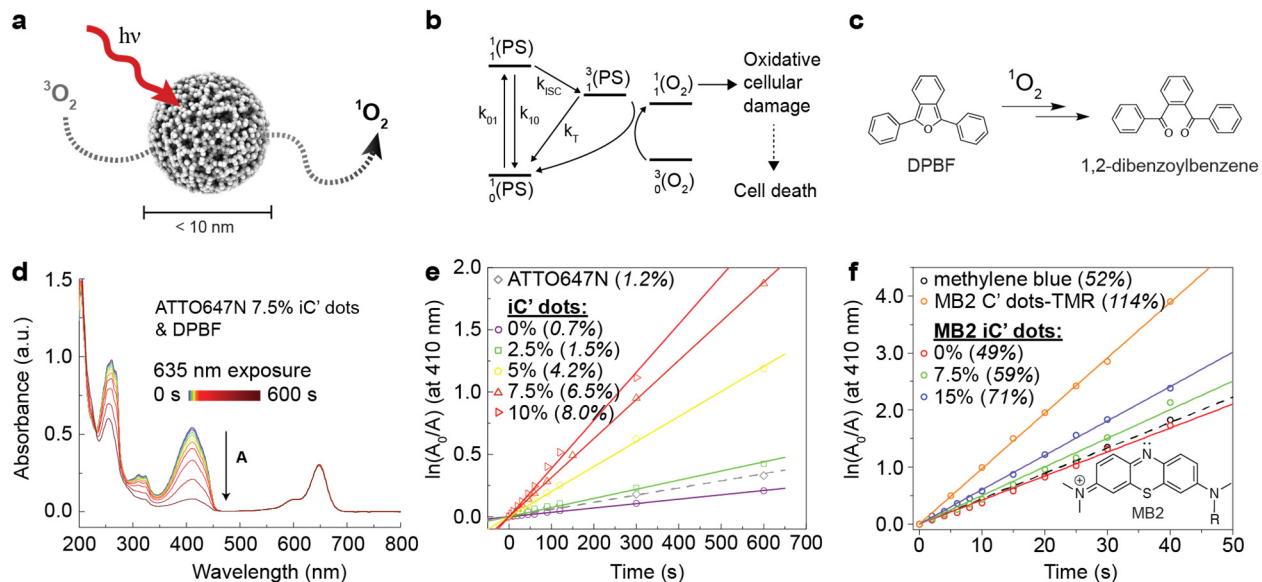


Figure 2. (a) Particle rendering with schematic of triplet oxygen, $^3\text{O}_2$, diffusing through the microporous silica network and being transformed into singlet oxygen, $^1\text{O}_2$, by encapsulated dyes under red light illumination. (b) Simplified Jablonski diagram illustrating the creation of singlet oxygen. $^0_1(\text{PS})$ denotes the singlet ground state, while $^1_1(\text{PS})$ and $^1_3(\text{PS})$ denote electronically excited singlet and triplet states of a dye photosensitizer (PS), respectively. $^0_3(\text{O}_2)$ and $^1_1(\text{O}_2)$ denote triplet ground state and excited singlet state of molecularly dissolved oxygen, respectively. (c) Singlet oxygen sensor 1,3-diphenylisobenzofuran (DPBF) and its reaction to 1,2-dibenzoylbenzene in the presence of $^1\text{O}_2$ (double arrow indicates two-step reaction). (d) Absorption spectra of a solution of ATTO647N encapsulating 7.5% iC'dots and DPBF, irradiated at 635 nm (ATTO647N absorption band) for 0 s to 600 s (black arrow). (e) Singlet-oxygen generation for ATTO647N dye (dashed line) as compared to ATTO647N encapsulating 0, 2.5, 5, 7.5 and 10 % iC'dots (solid lines). Values for Φ_Δ are in parentheses. (f) methylene blue dye (dashed line) as compared to MB2 encapsulating 0, 7.5, 15% iC'dots, and MB2 encapsulating C' dots with TMR surface functionalization (solid lines). Values for Φ_Δ are in parentheses. The inset of (f) shows the chemical structure of encapsulated methylene blue derivate MB2. R represents a functional group attached by a carbon atom.

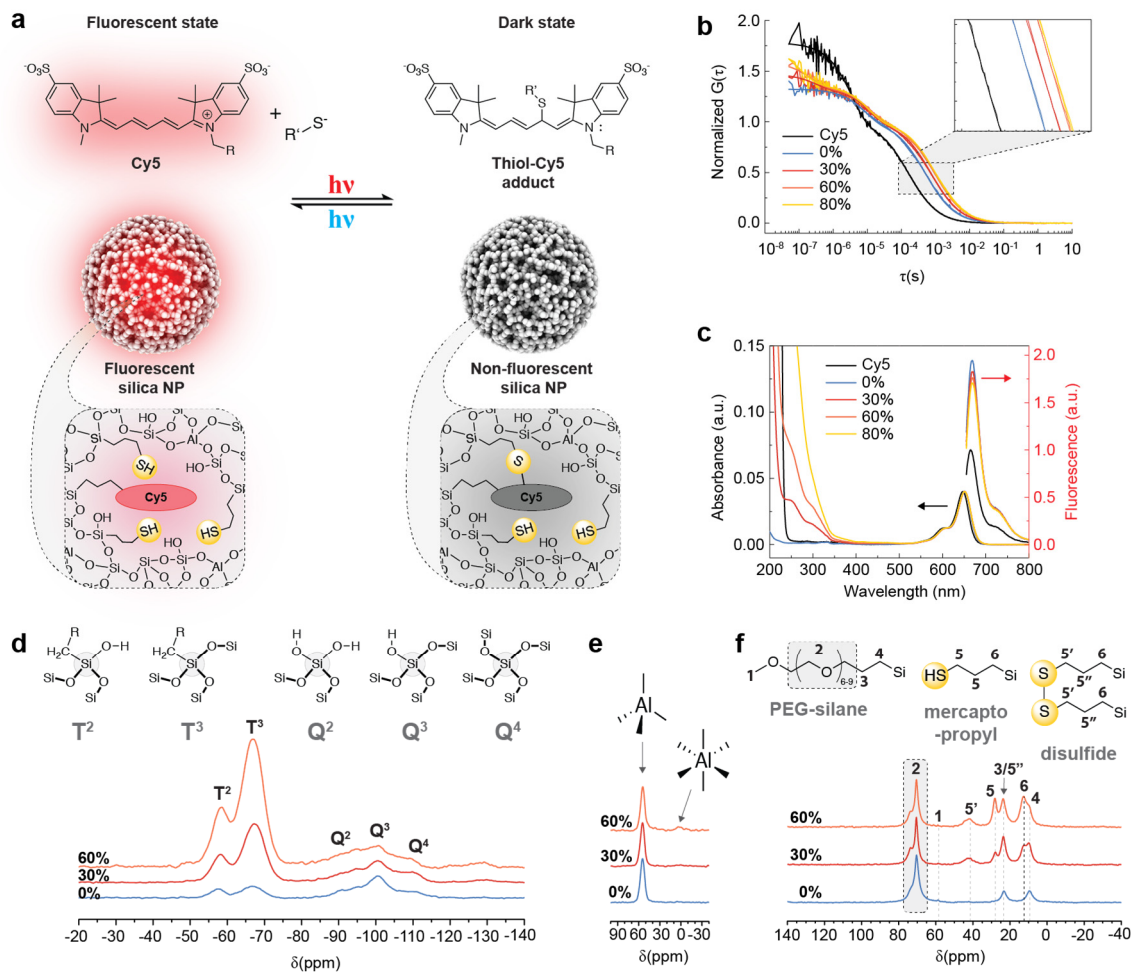


Figure 3. (a) Cy5 reversible photoswitching mechanism in the presence of thiol components from fluorescent state (left) to dark state (right) with corresponding particle rendering and local molecular structure models. R and R' represent functional groups attached by a carbon atom. (b) Normalized FCS autocorrelation curves of free Cy5 dye and various Cy5 srC' dots with increasing thiol content (0, 30, 60, and 80%). Corresponding fits used a correlation function with translational diffusion, cis-trans isomerization, and rotational diffusion components. (c) Corresponding intensity-matched absorption (left black arrow) and emission spectra (right red arrow) from 645 nm excitation. (d) Solid-state ^{29}Si CP/MAS NMR spectra of srC' dots (0, 30, and 60%) showing T- and Q-group assignments with structural illustrations. (e) Solid-state ^{27}Al MAS NMR spectra of srC' dots (0, 30, and 60%) with assignments to four- and six-fold coordinated aluminum. (f) Solid-state ^{13}C CP/MAS NMR spectra of srC' dots (0, 30, and 60%) with peak assignments to carbons from PEG-silane, mercaptopropyl, and disulfide groups. The peak of carbon position 5'' at 22 ppm is only partially visible as a high-field shoulder of the carbon peak of position 3.

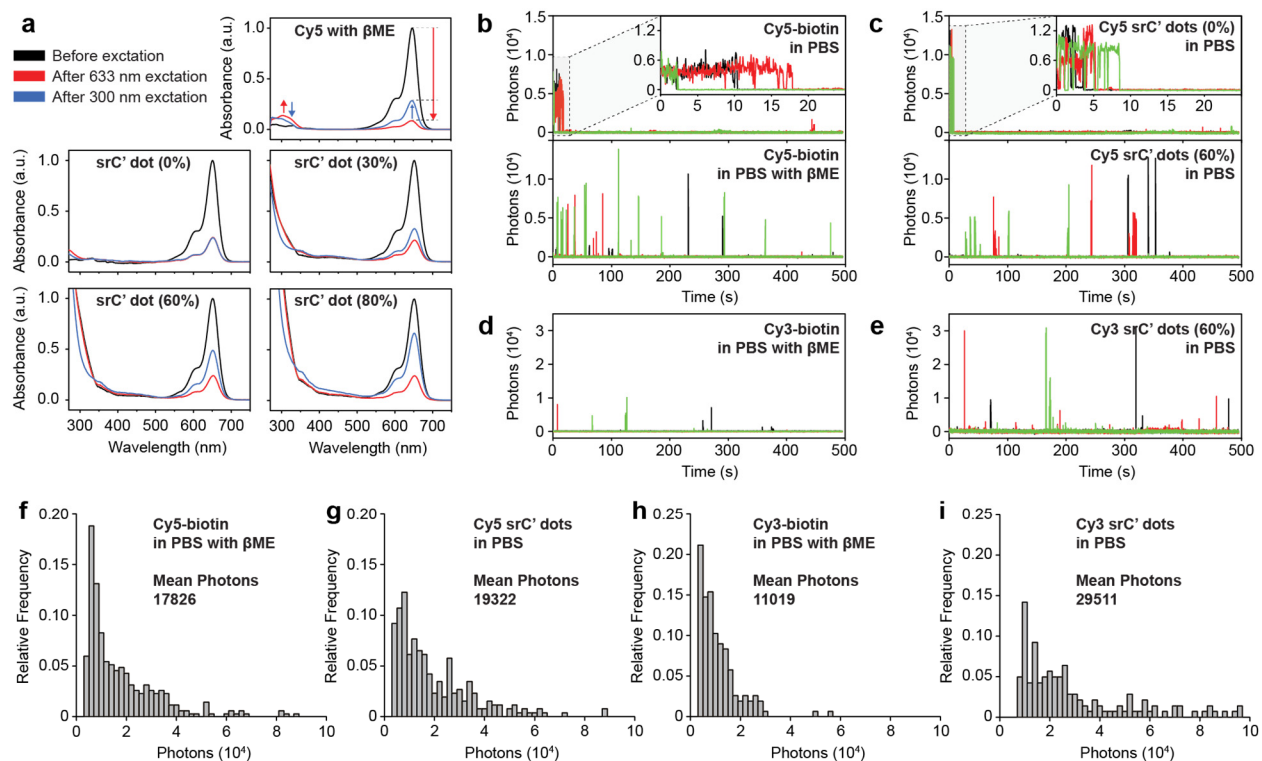


Figure 4. (a) Photoswitching absorption spectra, before excitation (black), after 30 min 633 nm light (red, arrows), and 5 min 300 nm light (blue, arrows) exposure, of Cy5 in DI water in the presence of β ME and different srC' dots (0, 30, 60, and 80%) in the absence of β ME. (b – e) Single molecule and single particle fluorescence traces recorded for different imaging buffer conditions with insets highlighting short time behavior in (b) and (c). Black, red, and green lines refer to three different fluorophores or particles. (f - i) Photon histograms of different dyes and particles for different imaging buffer conditions (as indicated).

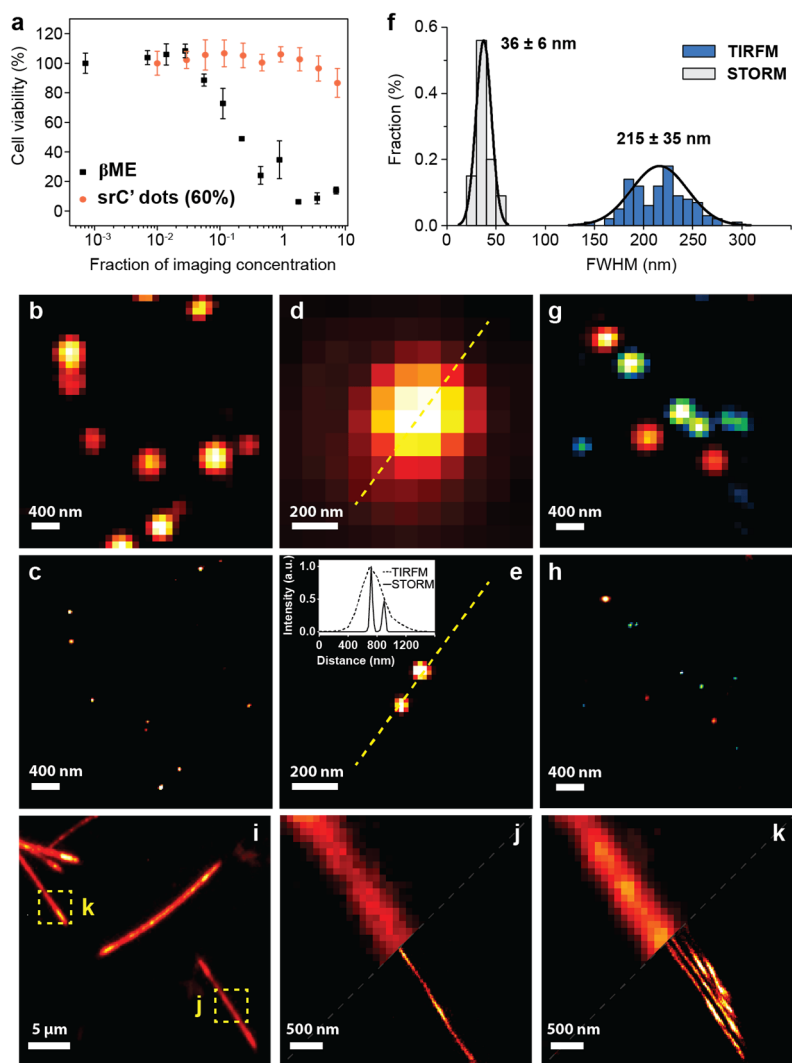


Figure 5. (a) Cell viability tests with BxPC3 cell line in complete media under the influence of β ME, 16 hours incubation, or Cy5 srC' dots (60%), 6 days incubation, at different concentrations, normalized to typical values used in STORM microscopy for comparative purposes as detailed in the text. Error bars represent the standard deviation from the mean of three independent experiments. (b) and (d) Total internal reflection fluorescence microscopy (TIRFM) images of Cy5 srC' dots (60%) in PBS in the absence of β ME. (c) and (e) Corresponding reconstructed super-resolution images. For yellow lines in (d) and (e) line intensity profiles are plotted in the inset of (e) revealing resolution enhancement for the reconstructed STORM image (solid line) over the diffraction limited TIRFM image (dashed line). (f) FWHM image analysis of TIRFM images and reconstructed super-resolution images from STORM. (g) Dual color TIRFM images of Cy5 srC' dots and Cy3 srC' dots in PBS in the absence of β ME, and (h) corresponding reconstructed super-resolution image. (i) TIRFM image of Cy5 srC' dots labeled microtubules. (j) and (k) SR images of a single microtubule and multiple parallel microtubules partially overlaid with conventional TIRFM images of selected areas from (i) (yellow boxes)

Supporting Information

Supporting Information is available from the Wiley Online Library or from the author.

Author Contributions

F.F.E.K. and J.A.H. contributed equally. F.F.E.K. and U.B.W. developed the experimental design. F.F.E.K. developed and synthesized nanoparticles, conducted and analyzed steady-state absorption and emission spectroscopy, FCS, EDS and ensemble photoswitching experiments. N.D. and S.L. helped with optimization and synthesis of nanoparticles. U.W-Z. and J.Z. acquired and analyzed ssNMR data. S.L. performed singlet oxygen quantum yield measurements. J.A.H., F.F.E.K., and J.A.E. carried out microscopy measurements and photon statistical analysis. Cell studies were carried out by W.P.K. All authors were involved in data interpretation and discussion. F.F.E.K., J.A.H, and U.B.W. prepared the manuscript.

Acknowledgements

This work was funded by the Department of Energy, Office of Science, Basic Energy Sciences, under Award No. DE-SC0010560. J.A.H. thanks the National Institutes of Health (NIH) for financial support under Award No. U54CA199081. J.A.E. would like to thank the Alfred P. Sloan Foundation's Minority Ph.D. Program for financial support. This work made use of the Cornell Center for Materials Research (CCMR) shared facilities which are supported through the NSF MRSEC program (DMR-1719875) at Cornell. Imaging data was acquired through the Cornell University Biotechnology Resource Center, with NSF funding (DBI-1428922) for the shared Zeiss Elyra Microscope. R.A.C. and W.P.K. acknowledge funding from the National Institutes of Health (GM122575, CA201402, CA210184). The authors gratefully acknowledge B. Baird, W. Zipfel and R. Williams (Cornell University) for helpful discussion and kind

experimental assistance.

Conflict of Interest

A patent disclosure of this work has been submitted to the Center for Technology Licensing (CTL) at Cornell University. U.W. and Cornell have a financial interest in Elucida Oncology, Inc.

References

- [1] Y. Tokura, M. Kawasaki, N. Nagaosa, *Nat. Phys.* **2017**, *13*, 1056.
- [2] L. E. Brus, *J. Chem. Phys.* **1984**, *80*, 4403.
- [3] J. A. Mundy, C. M. Brooks, M. E. Holtz, J. A. Moyer, H. Das, A. F. Rébola, J. T. Heron, J. D. Clarkson, S. M. Disseler, Z. Liu, A. Farhan, R. Held, R. Hovden, E. Padgett, Q. Mao, H. Paik, R. Misra, L. F. Kourkoutis, E. Arenholz, A. Scholl, J. A. Borchers, W. D. Ratcliff, R. Ramesh, C. J. Fennie, P. Schiffer, D. A. Muller, D. G. Schlom, *Nature* **2016**, *537*, 523.
- [4] C. R. Kagan, C. B. Murray, *Nat. Nanotechnol.* **2015**, *10*, 1013.
- [5] J. Wang, B. Wylie-Van Eerd, T. Sluka, C. Sandu, M. Cantoni, X. K. Wei, A. Kvasov, L. J. McGilly, P. Gemeiner, B. Dkhil, A. Tagantsev, J. Trodahl, N. Setter, *Nat. Mater.* **2015**, *14*, 985.
- [6] C. Broholm, I. Fisher, J. Moore, M. Murnane, **2017**, *1*.
- [7] R. K. Iler, *The chemistry of silica: solubility, polymerization, colloid and surface properties, and biochemistry*; **1979**.
- [8] W. E. Moerner, Y. Shechtman, Q. Wang, *Faraday Discuss.* **2015**, *184*, 9.
- [9] J. C. Koziar, D. O. Cowan, *Acc. Chem. Res.* **1978**, *11*, 334.

- [10] M. Kasha, *J. Chem. Phys.* **1952**, *20*, 71.
- [11] S. S. Lucky, K. C. Soo, Y. Zhang, *Chem. Rev.* **2015**, *115*, 1990.
- [12] S. Bretschneider, C. Eggeling, S. W. Hell, *Phys. Rev. Lett.* **2007**, *98*.
- [13] K. Ma, C. Mendoza, M. Hanson, U. Werner-Zwanziger, J. Zwanziger, U. Wiesner, *Chem. Mater.* **2015**, *27*, 4119.
- [14] K. Ma, D. Zhang, Y. Cong, U. Wiesner, *Chem. Mater.* **2016**, *28*, 1537.
- [15] J. Widengren, P. Schwillé, *J. Phys. Chem. A* **2000**, *104*, 6416.
- [16] D. R. Larson, H. Ow, H. D. Vishwasrao, A. A. Heikal, U. Wiesner, W. W. Webb, *Chem. Mater.* **2008**, *20*, 2677.
- [17] J. Widengren, Ü. Mets, R. Rigler, *J. Phys. Chem.* **1995**, *99*, 13368.
- [18] A. Chmyrov, T. Sandén, J. Widengren, *J. Phys. Chem. B* **2010**, *114*, 11282.
- [19] G. S. Engel, T. R. Calhoun, E. L. Read, T. K. Ahn, T. Mančal, Y. C. Cheng, R. E. Blankenship, G. R. Fleming, *Nature* **2007**, *446*, 782.
- [20] E. Thyryhaug, R. Tempelaar, M. J. P. Alcocer, K. Židek, D. Bína, J. Knoester, T. L. C. Jansen, D. Zigmantas, *Nat. Chem.* **2018**, *10*, 780.
- [21] S. Kim, T. Y. Ohulchanskyy, D. Bharali, Y. Chen, R. K. Pandey, P. N. Prasad, *J. Phys. Chem. C* **2009**, *113*, 12641.
- [22] L. Zhou, S. Wei, X. Ge, J. Zhou, B. Yu, J. Shen, *J. Phys. Chem. B* **2012**, *116*, 12744.
- [23] E. Phillips, O. Penate-Medina, P. B. Zanzonico, R. D. Carvajal, P. Mohan, Y. Ye, J. Humm, M. Gonen, H. Kalaigian, H. Schoder, H. W. Strauss, S. M. Larson, U. Wiesner, M. S. Bradbury, *Sci. Transl. Med.* **2014**, *6*, 260ra149.
- [24] A. B. Ormond, H. S. Freeman, *Materials (Basel)*. **2013**, *6*, 817.

- [25] K. Ma, U. Wiesner, *Chem. Mater.* **2017**, *29*, 6840.
- [26] M. Heilemann, E. Margeat, R. Kasper, M. Sauer, P. Tinnefeld, *J. Am. Chem. Soc.* **2005**, *127*, 3801.
- [27] M. Heilemann, S. Van De Linde, A. Mukherjee, M. Sauer, *Angew. Chemie - Int. Ed.* **2009**, *48*, 6903.
- [28] G. T. Dempsey, M. Bates, W. E. Kowtoniuk, D. R. Liu, R. Y. Tsien, X. Zhuang, *J. Am. Chem. Soc.* **2009**, *131*, 18192.
- [29] M. J. Rust, M. Bates, X. Zhuang, *Nat. Methods* **2006**, *3*, 793.
- [30] M. Fernández-Suárez, A. Y. Ting, *Nat. Rev. Mol. Cell Biol.* **2008**, *9*, 929.
- [31] K. White, J. V. Bruckner, W. L. Guess, *J. Pharm. Sci.* **1973**, *62*, 237.
- [32] H. M. Kao, P. J. Chiu, G. L. Jheng, C. C. Kao, C. T. Tsai, S. L. Yau, H. H. G. Tsai, Y. K. Chou, *New J. Chem.* **2009**, *33*, 2199.
- [33] G. T. Dempsey, J. C. Vaughan, K. H. Chen, M. Bates, X. Zhuang, *Nat. Methods* **2011**, *8*, 1027.
- [34] C. E. Shannon, *Proc. IRE* **1949**, *37*, 10.
- [35] S. Van De Linde, A. Löschberger, T. Klein, M. Heidbreder, S. Wolter, M. Heilemann, M. Sauer, *Nat. Protoc.* **2011**, *6*, 991.
- [36] M. Ovesný, P. Křížek, J. Borkovec, Z. Švindrych, G. M. Hagen, *Bioinformatics* **2014**, *30*, 2389.
- [37] T. Kao, F. Kohle, K. Ma, T. Aubert, A. Andrievsky, U. Wiesner, *Nano Lett.* **2018**, *18*, 1305.
- [38] K. I. Mortensen, L. S. Churchman, J. A. Spudich, H. Flyvbjerg, *Nat. Methods* **2010**, *7*, 377.